GSA DATA REPOSITORY 2012125

An atmospheric origin of Martian Interior Layered Deposits (ILDs): Links to climate change and the global sulfur cycle

Joseph R. Michalski and Paul. B. Niles

Methods

OMEGA data were processed into atmospherically corrected I/F spectra using standard techniques described previously (Poulet et al., 2007). Each image cube was processed into two types of spectral index map: a 2.1 μm index (BD21) tuned to identify monohydrated sulfates(Mangold et al., 2008) and a 2.4 μm index (BD24) that identifies polyhydrated sulfates (Griffes et al al., 2007; Roach et al., 2010; Wiseman et al., 2010). Both of these spectral index maps were used together to map occurrences of sulfates within Ophir, Candor, and Melas Chasmata and no distinction is made between the two classes of sulfates in this work. Sulfate-bearing units were identified where >5 contiguous pixels (though most include >>5) above the detection limit of either index occur together (Figure 1). Detections were validated by comparison to previous work showing localized sulfate detections and by inspection of extracted surface spectra for evidence of sulfate minerals. The area and average elevation of each mapped deposit was calculated using a Geographic Information System (GIS).

We estimated the volume of Valles Marineris shown in Figure 1 by transforming MOLA gridded altimetry data into a Triangulated Irregular Network (TIN), fitting a plane to the elevation of L2, and calculating the volume below this plane. This estimate is then added to the estimated volume of the modern day ILDs (in their eroded, current configuration) that was published previously (Hynek et al., 2003).

Sulfur Outgassing

The range of estimated volcanic outgassing of SO_2 cited in the paper is derived from estimates of outgassing by period on Mars by Craddock and Greeley (2009) as a lower bound and a calculation combining the crustal production model of Hirschmann and Withers (2008) with SO_2 solubility experiments by Righter et al. (2009) as an upper bound.

The estimates of Craddock and Greeley are considered minimum estimates because a) they rely on observed volcanic deposits in calculating volumes of volcanic materials and linking those to volcanic outgassing (thereby potentially omitting intrusive bodies that might have contributed to the atmosphere or earlier volcanics that may have been eroded or buried and thereby erased from the geologic record), and b) they specifically ignore numerous small vents dotting the landscape that would have contributed to the outgassed budgets, albeit in small volumes.

On the other hand, crustal production models provide the largest estimates of volcanic output on Mars since they do not distinguish between intrusive and extrusive volcanism and include volcanic output during the early Noachian when volcanic activity was likely to be the highest. We utilize the crustal production model of Hirschmann and Withers (2008) (Figure DR1) to estimate magmatic output through martian history.

The amount of sulfur degassed by a specified amount of magma is also a complex issue. Most studies have used estimates based on terrestrial volcanism, or other speculation. The issue has been treated experimentally by Righter et al. (2009) who estimate an average 2400 ppm sulfur to be degassed from sulfide saturated martian magmas. This is an upper bound assuming that all magmas are sulfide saturated, this is likely not the case and estimates of terrestrial degassing are close to this and usually below this value. Thus the upper bounds on sulfur outgassing are calculated by combining igneous crust production volumes over time from Hirschmann and Withers (2008) (Figure DR1) with estimates of magmatic sulfur content from Righter et al. (2009) (0.24% SO_3).

In order to calculate amount of SO_2 degassed during each period of history we adapted the results of Craddock and Greeley (2009) by normalizing to 100 My to account for the difference in length of each period in Martian history. Absolute dates taken to represent the end of each period are as follows: Late Amazonian (0), Middle Amazonian (500 Ma), Early Amazonian (2 Ga), Late Hesperian (3 Ga), Early Hesperian (3.5 Ga), Late Noachian (3.7 Ga), Mid-Noachian (3.9 Ga), Early Noachian (4.2). The upper bound was calculated by using the modeled crustal production from Hirschmann and Withers (2008) for the time periods specified above.

The Canyon-Fill Scenario

The presence of massive mounds of altered material in the canyon system is striking and must be accounted for. Figure DR2 shows a cross section through Melas and Candor Chasmata and the topographic distribution of altered ILDs along that profile. If the materials were altered by groundwater, then it must be that groundwater had enough hydraulic head to reach a high level in the canyon. Given that the canyon system consists of open basins, that water was unlikely to occur within lakes or seas. That issue has prompted previous authors to conclude that groundwater-saturated sediment was present in the canyon up to the necessary level.

Two hypothetical models to explain the origin of ILDs are shown in Figure DR3. Each is in progressive time-steps from T1 to T4. In the groundwater-driven/canyon fill model, the vast topographic basin of the canyon depresses the groundwater table. Successive infilling of the canyon by sediment allows groundwater to exist at progressively higher levels. Groundwater-altered canyon-fill sediments are then eroded to their current configuration. In the atmospheric driven model, some groundwater exists but it is not a key mechanism. Instead, pyroclastic and other particulate materials fall into the canyon and are altered by acidic snow and ice from atmospheric sources. Successive events create draping relationships and crude compositional stratigraphy. The same scenario can explain sulfate-bearing layered sediments of similar age on the plains outside the canyon.

Obliquity-Driven Ice Deposition

Madeleine et al. (2009) note that thermal inertia is an important factor in their climate modeling procedures. As such, areas with high thermal inertia result in lower summertime sublimation rates and higher net accumulation. They point out that this may be a real and important effect of the surface on ice accumulation, but also, that it could lead to biases if the present day thermal inertia is different from what would have existed in the past. For example, the thermal inertia of the Valles Marineris is generally high, and so these areas could be biased toward higher ice accumulation if the past thermal inertia of the surface was much less than it is today. However, there is no reason to assume that the thermal inertia of the surface was in fact much lower in the past in the canyon system than it is today. We consider this to be an open question to explore further in future work.

References

Griffes, J. L., Arvidson, R. E., Poulet, F., and Gendrin, A., 2007, Geologic and spectral mapping of etched terrain deposits in northern Meridiani Planum: Journal of Geophysical Research-Planets, v. 112, no. E8.

Poulet, F., Gomez, C., Bibring, J. P., Langevin, Y., Gondet, B., Pinet, P., Belluci, G., and Mustard, J., 2007, Martian surface mineralogy from Observatoire pour la Mineralogie, l'Eau, les Glaces et l'Activite on board the Mars Express spacecraft (OMEGA/MEx): Global mineral maps: Journal of Geophysical Research-Planets, v. 112, no. E8.

Roach, L. H., Mustard, J. F., Swayze, G., Milliken, R. E., Bishop, J. L., Murchie, S. L., and Lichtenberg, K., 2010, Hydrated mineral stratigraphy of Ius Chasma, Valles Marineris: Icarus, v. 206, no. 1, p. 253-268.

Wiseman, S. M., Arvidson, R. E., Morris, R. V., Poulet, F., Andrews-Hanna, J. C., Bishop, J. L., Murchie, S. L., Seelos, F. P., Des Marais, D., and Griffes, J. L., 2010, Spectral and stratigraphic mapping of hydrated sulfate and phyllosilicate-bearing deposits in northern Sinus Meridiani, Mars: Journal of Geophysical Research-Planets, v. 115.

FIGURE DR1

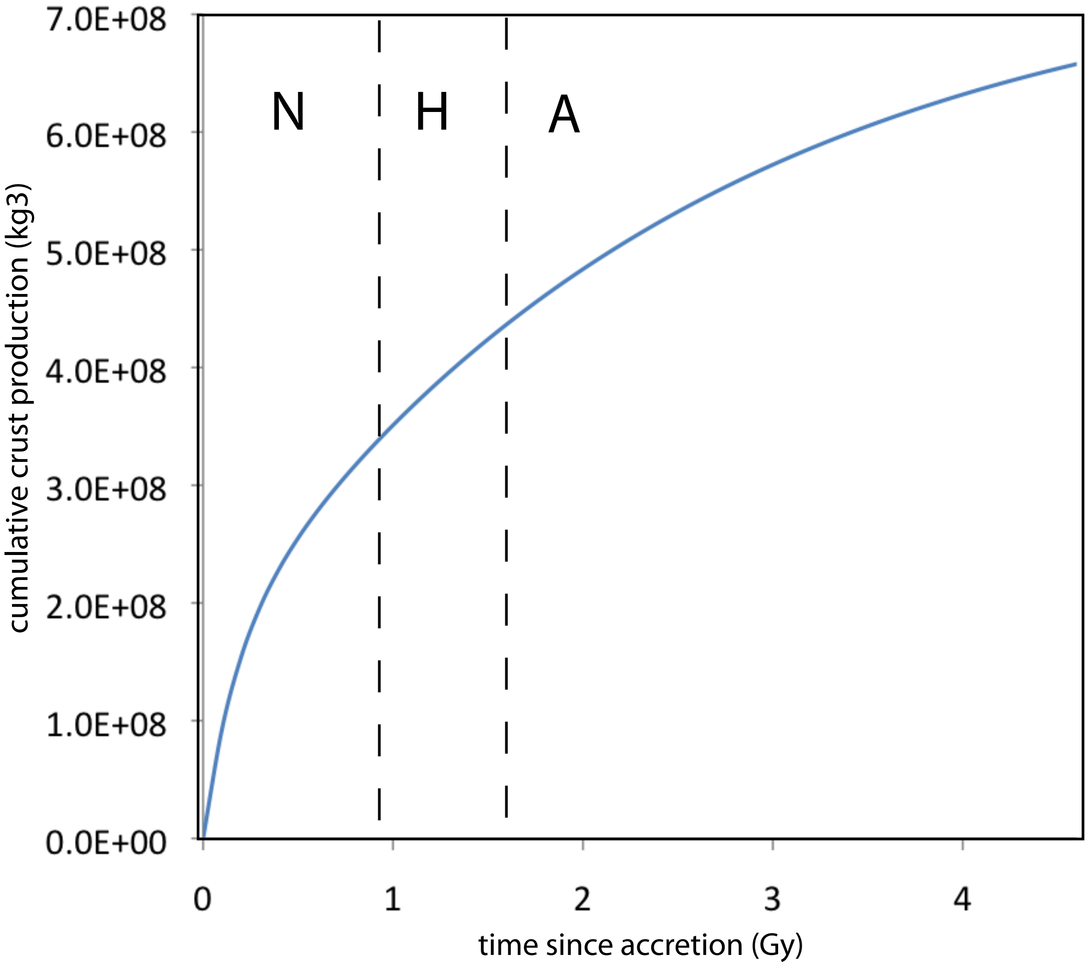

7.0E+08
6.0E+08
5.0E+08
4.0E+08
3.0E+08
2.0E+08
1.0E+08
0.0E+00
cumulative crust production (kg3)
0
1
2
3
4
time since accretion (Gy)
N
H
A

FIGURE DR2

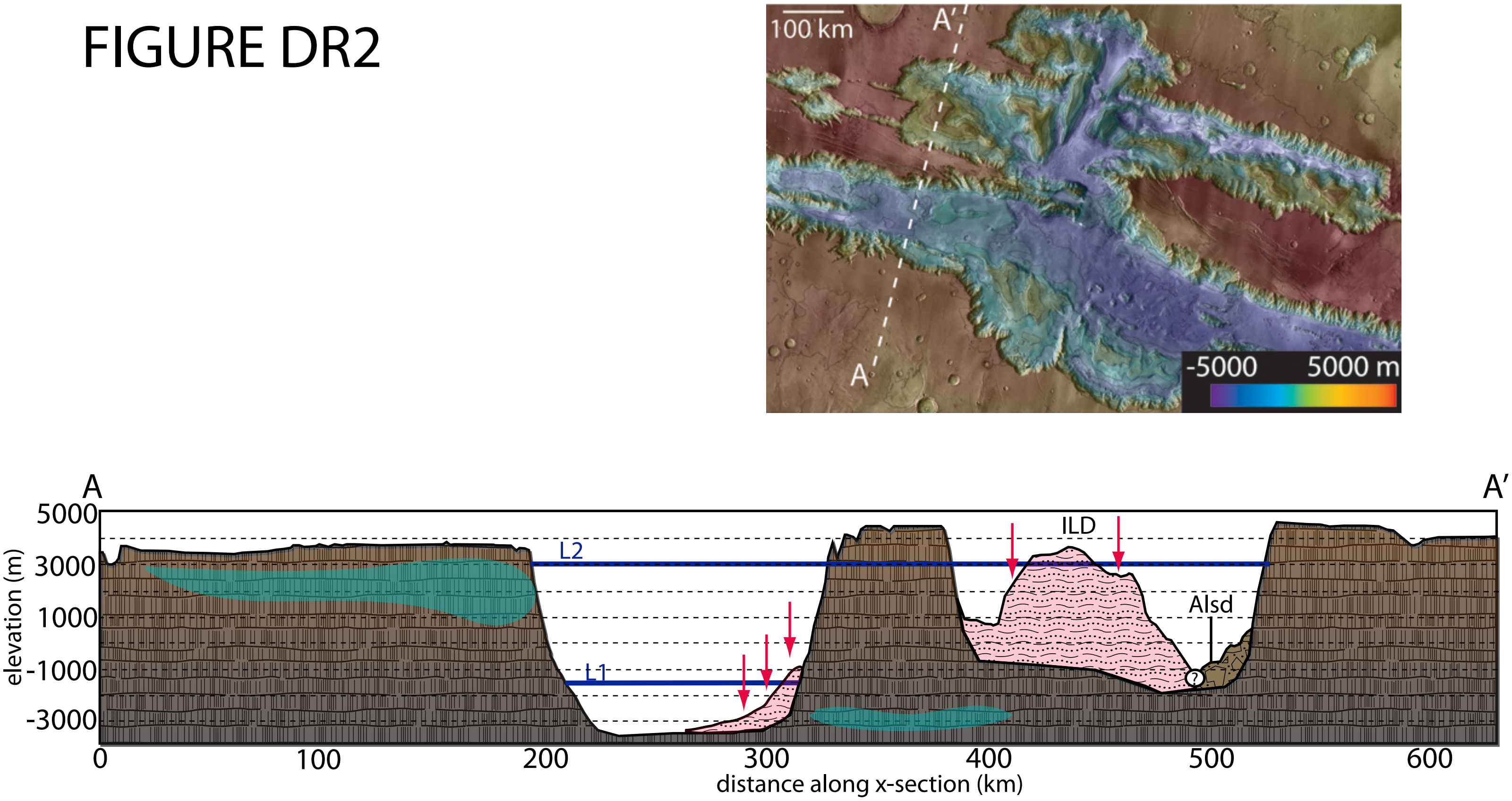

100 km
A′
A
-5000
5000 m
A
A′
5000
3000
1000
-1000
-3000
elevation (m)
L2
L1
ILD
Alsd
?
0
100
200
300
400
500
600
distance along x-section (km)

FIGURE DR3

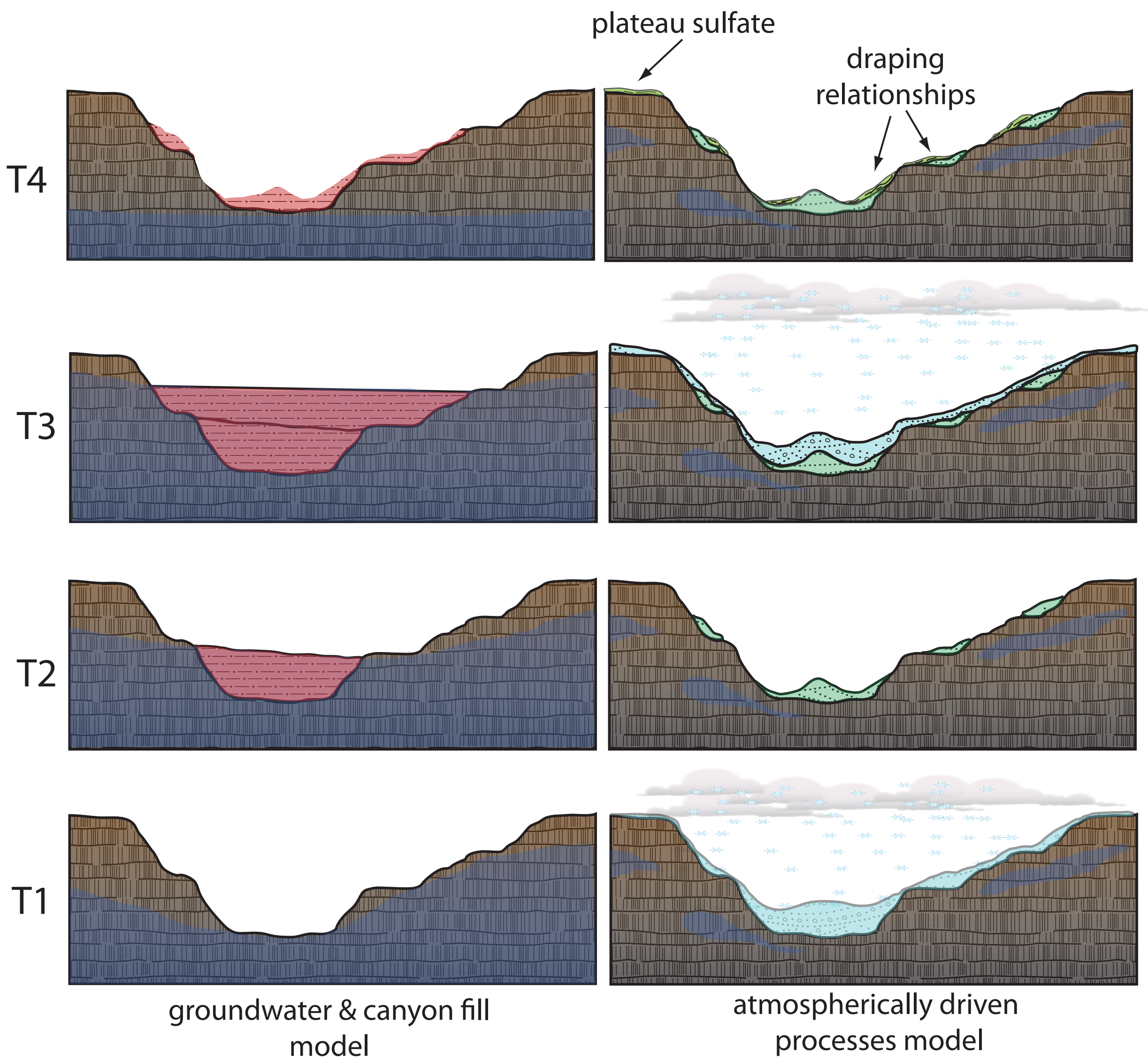

plateau sulfate
draping relationships
T4
T3
T2
T1
groundwater & canyon fill model
atmospherically driven processes model